Internal stability improvement of a natural gas centrifugal compressor system based on a new optimal output feedback controller using block transformation and grey wolf optimizer

Bachir Nail [a,*], Belkacem Bekhiti [b], Vicenç Puig [c]

[a] Mechanical Engineering, Materials and Structures Laboratory, Institute of Science and Technology, Tissemsilt University Center, Tissemsilt, Algeria
[b] Institute of Aeronautics and Space Studies, Saad Dahlab University, Blida, Algeria
[c] Automatic Control Department, Universitat Politécnica de Catalunya (UPC), TR11, Rambla de Sant Nebridi, 10, 08222, Terrassa, Spain

ARTICLE INFO

Keywords:
Centrifugal compressor
Internal stability
Output-feedback
Canonical block transformation
Grey wolf optimizer
Surge phenomenon

ABSTRACT

The improvement of the normal operating mode in gas compression systems performs an essential role in enhancing the process of pumping and transporting the natural gas inside and outside the border of Algeria. In this regards, this paper introduces a novel output-feedback controller design with optimal static matrix gains K, which uses to control and maintain its internal stability by reducing the surge phenomenon appeared clearly in the thermodynamical outputs parameters of the studied centrifugal compressor system. The feedback matrix K is calculated based on transforming the dynamical model using the similarity canonical block transformation (CBT) and determining the block own matrix $\mathscr{F}_{own}$ by using the famous grey wolf optimizer (GWO). In given view of this study, a comparative investigation carried out, using different optimization methods, and two recent algorithms, to attest the advantages of the proposed controller. The obtained results confirm the internal stability robustness in the presence of disturbances and uncertainty of the system parameters up to 50%. The obtained norm of the proposed controller is $||K|| = 0.69$, which guarantees a comfortable interval of internal stability in closed loop system (CLS), stability interval = **[0.26, 0.60]** with minimum possible energy. The three stability measures of compressor system is still ensured comparing with other algorithms **[0.0171, 0.0012, 0.0276]**. The proposed controller eliminates the fluctuation in the outputs of the studied system, the discharge pressure (P2) and the discharge temperature (T2), respectively, i.e. the disappearance of the surge phenomenon completely. We mention that the proposed controller is suitable and applicable only in the parametric and the transformable models.

1. Introduction

The compressors are devices that transform the mechanical energy supplied by a motive machine into pressure energy; (by increasing the pressure of a gaseous fluid). The centrifugal compressor systems use in various fields such as: the exploitation, transportation and treatment of natural gas, the mechanical metallurgy, and in aerospace propulsion, etc. The benefits of these machines are that they can be coupled directly to a turbine or electric motor without a rod-crank mechanism. It is, for this reason, are less bulky compared to piston compressors. (Zhang, 2016), (Liu et al., 2019), (Agney et al., 2018), (Niknam et al., 2018), (Meroni et al., 2018), (Marjani and Baghmolai, 2016) and (Eker and Kara, 2003). Consequently, a reasonable comprehension control of these systems is necessary to enhance their productivity and reduce their operating cost. In this case, one of the weaknesses in these systems determined by the internal dynamic stability problems due to the famous phenomenon pumping. For this reason considered an excellent target of application and examination to confirm the efficacy of the proposed controller. The investigated centrifugal gas compressor in this study is BCL 505, installed in the biggest gas field for natural gas compression in the south of Algeria. The operating behaviour modelling of the studied compressor system has been made based on experimental data obtained in situ, where the system have two aspirations inputs pressure (P1) and temperature (T1) and two discharge outputs pressure (P2) and temperature (T2) (Nail et al., 2018) and (NailAbdellah et al., 2019). Two comparative examinations have been carried by the

* Corresponding author.
E-mail address: bachir.nail@cuniv-tissemsilt.dz (B. Nail).

obtained results, for aim choose the best parameters of the feedback matrix gains K, first with three famous optimization algorithms, and second with two robust controllers published in recent years (Řezáč and Hurák, 2013) and (Veselý, 2001). We introduce in this study a novel static output-feedback controller K, which can implement into the large dimension complex systems. The design idea was inspired by finding a feedback action that might develop the performance of the studied system and can adjust the outputs parameters of the studied system systematically. The CBT features provide mathematical tools to embody the idea of this design by using CBT similarity in both left and right on sides of the studied system. After this step, the determine of the controller matrix gains K is limited to a small part called own block matrix $\mathscr{F}_{own}(\theta)$. Thus, the significant percentage of the output-feedback dynamics identified prior without calculation. To determine K permanently, should select the matrix $\mathscr{F}_{own}(\theta)$ in a way guaranteeing the global internal stability of the studied system with optimal energy (minimization the norm of K) taking in consideration some constraints related by the uncertainties in the parameters, in this regards the recent GWO (Mirjalili et al., 2014), is used to solve this optimization problem. In modern control of complex systems, the states variables are not measurable and available at all the time. Possibly it is hard and expensive (the price of sensors) to have the measurement of the whole state vector, or for theoretical and design problems. For this end, various control algorithms stated in the literature using the output information uniquely, to regulate the parameters of industrial systems. The design of this class of controllers is complicated in control engineering, and be a challenge from a technical and mathematical point of view. Furthermore, it is befalling in the NP-hard category. Many control problems design can be put in the form of convex optimization programming. The principal interest of this type of optimization is the capability of guaranteeing the global minimum. The basic tool for solving the resulting design problem is the use of the linear matrix inequalities (LMIs). LMIs are increasingly used for solving many problems in control theory (Chesi and Middleton, 2018). Among the reasons for its success, the existence of effective numerical resolution methods (with polynomial cost), the possibility to reformulate many problems of analysis, (stability, certain performances, etc.), in terms of LMIs, the ability to deal with problems with uncertain parameters, which played a big role in the development of the robust control theory and its application in these last years. Several recent published papers proposed new efficient algorithms, most based on the use of the (LMIs) tools, able to provide a practical solution to the output-feedback stabilization control design problem. As example, the following references are provided: an improved iterative LMI method for SOF control with application to MIMO PID controller (He and Wang, 2006), output feedback stabilization based on LMI for a continuous and/or discrete-time system with and without time delay (He et al., 2008) and (Duan and Hao, 2015), output-feedback controller of Takagi-Sugeno fuzzy-model based on LMI (Ho Jae Lee and Do Wan Kim, 2009), among other. Also, some approaches have proposed the combination of the LMI and optimization (H_∞ or H_2), or the meta-heuristic algorithms, among them: (H_∞ or H_2) output-feedback controller design based on LMI (Rubió-Massegú et al., 2014), (Fujimori, 2004), (Wei et al., 2018), (Gadewadikar et al., 2007), (Estrada--Manzo et al., 2019) and (Wu et al., 2019), the hybrid approach based on GA and LMI algorithms such as: controller-design for building using output-feedback taking in consideration the actuator saturation (Du and Lam, 2006), regional Takagi-Sugeno using mixed approaches based on output-feedback fuzzy-controller design (Chung and Wu, 2009), and robust output-feedback design against sensor fault applied on vehicle dynamics (Aouaouda et al., 2014), and other algorithms (Palacios-Quiñonero et al., 2014a), (Palacios-Quiñonero et al., 2014b), (Nguyen et al., 2018) and (Dong and Yang, 2013). Revising the existing approaches to solve the design of output-feedback controller problems, we can realize that most are solved based on optimization and computational tools.

2. The centrifugal compressor system: problem description of internal stability

2.1. The examined centrifugal gas compressor system of type BCL 505

Hassi R'Mel natural gas field is the most abundant field in southern Algeria. This field subdivided into three principal exploitation sections; each section includes several central pump stations, gas processing unities, group of gas turbine and centrifugal gas compressor systems. The production of this gas field, reaches 12×10^6 tons of condensate gas, 3.5×10^6 tons of LNG, and 10^{11} m^3 of dry natural gas, the primary elements of LNG is shown in Fig. 1, (NailAbdellah et al., 2019).

The leading role of the gas compression stations is to continually pump the dry gas to keep the demanded pressure level in national and the international market. The centrifugal gas compressor is driven by a gas turbine (GE-MS5002C) system, as shown in Fig. 2, each couple of turbine and compressor forms a compression line. The compression process carried out through two stages, the low-pressure and the high-pressure stages, where a cooling system based on air coolers used to regulate the temperature at the intermediary of the two stages (NailAbdellah et al., 2019).

A centrifugal compressor is a powerful machine with continuous fluid flow. Wheels attached to the shaft provide energy to the latter. A part of this energy transformed into an increased pressure moves directly in the wheels, and the rest in the stator (diffusers). This type of machine consists of an external body containing the part of the stator called the collection of diaphragms into which a rotor formed by the shaft, the wheels, the balancing piston and the collar of the thrust bearing. The rotor driven by the prime mover rotates the load bearings and guided in its axial position, the thrust bearing. The understanding the process operation of these machines is imperative to increase their production efficiency and reduce their rate of malfunctions. The centrifugal compressor investigated in this paper is shown in Fig. 3, and its physical properties are presented in Appendix A Table 6 (NailAbdellah et al., 2019).

The studied centrifugal compressor system designed by Nuovo Pignone company addressed for heavy applications such as gas pumping and transport stations. This system equipped by a control room contains a Distributed Control System (DCS) which allows acquisition inputs/outputs measurements data immediately from the installed sensors in the system. The principal function of the studied compressor is to guarantee the pressure surge of gas by a constant flow based on dynamic energy (NailAbdellah et al., 2019). The evaluation of compressor system performance usually not restricted within the single operation characteristic point, in Fig. 4 (a) a description of the rate compression in the

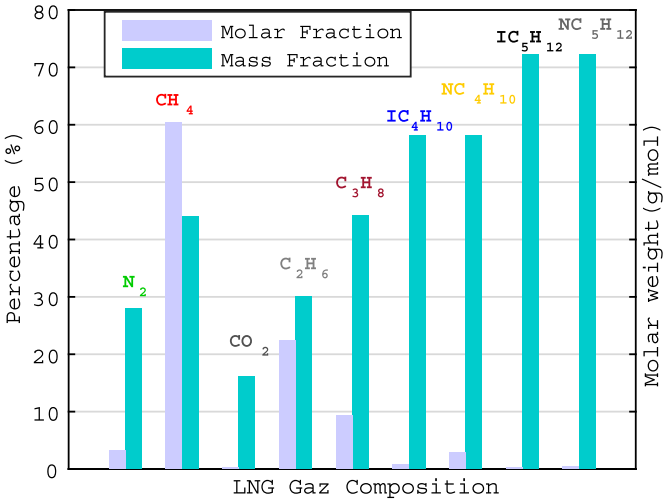

Fig. 1. LNG features and elements of Hassi R'Mel gas field.

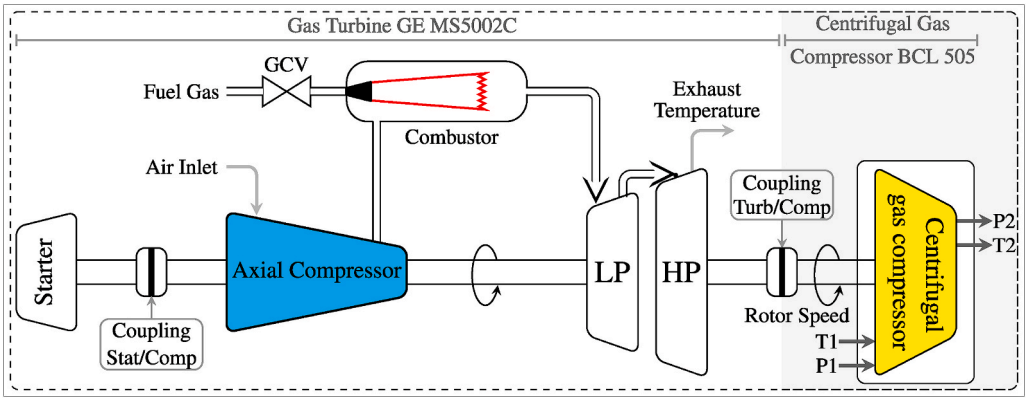

Fig. 2. MS GE 5002 gas turbine drive the studied BCL 505 centrifugal gas compressor system.

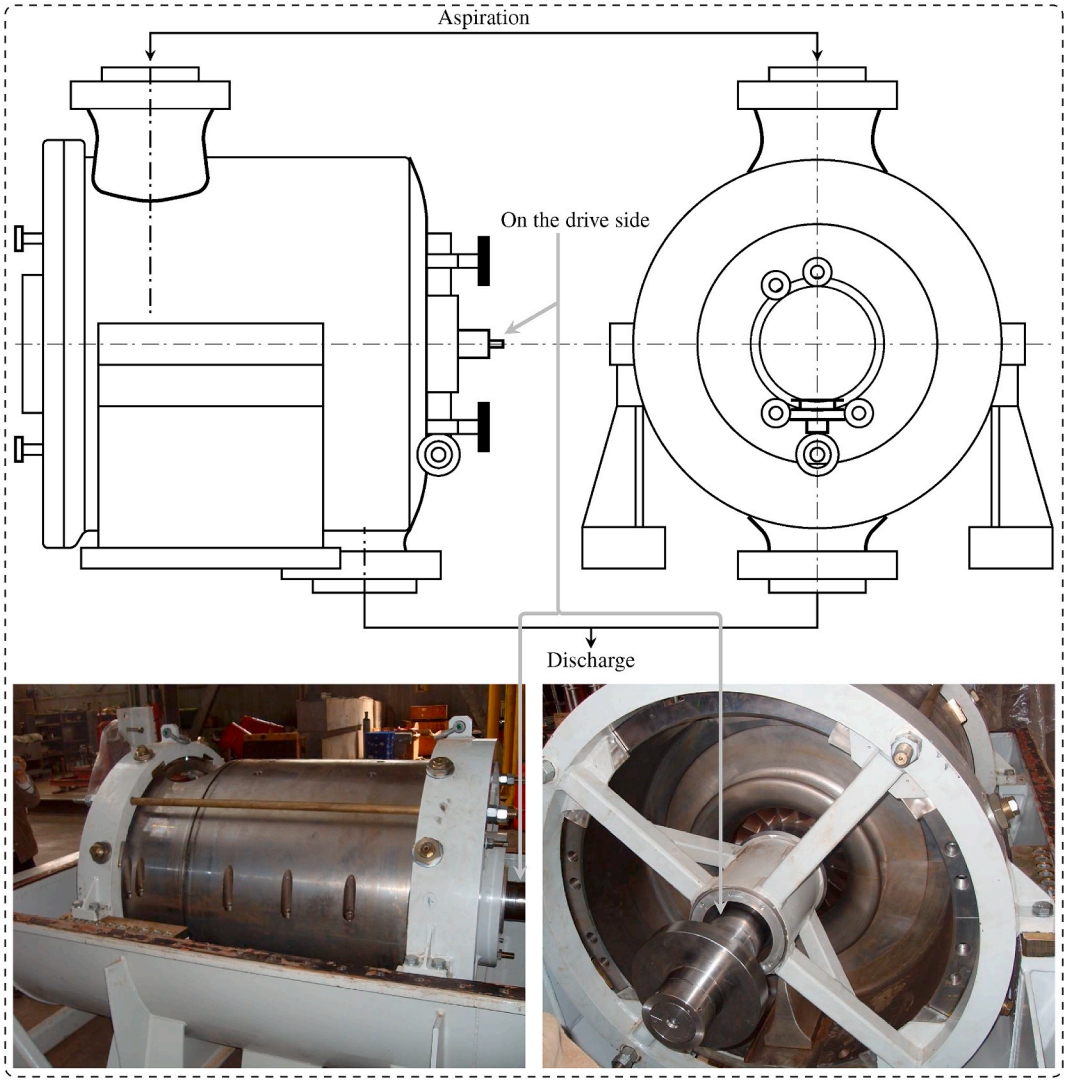

Fig. 3. The body of BCL 505 centrifugal gas compressor, with a practical show in the vertical joint plane.

function of the corrected rate of rotation speed. In the event of the low flows rates of pumping, a famous problem appear in compressor systems, called **surge phenomena**, which is characterized by the flow instability, followed by pressure waves of high amplitude, which can ultimately degrade the system (We talk about it in detail, in the next part of the problem description). In high flows of pumping, a blockage occurs, with a vibration phenomenon appeared in the floor section. Fig. 4 (b) shows the thermodynamics cycle of isentropic efficiency of the studied system, designed by the second principle of thermodynamics.

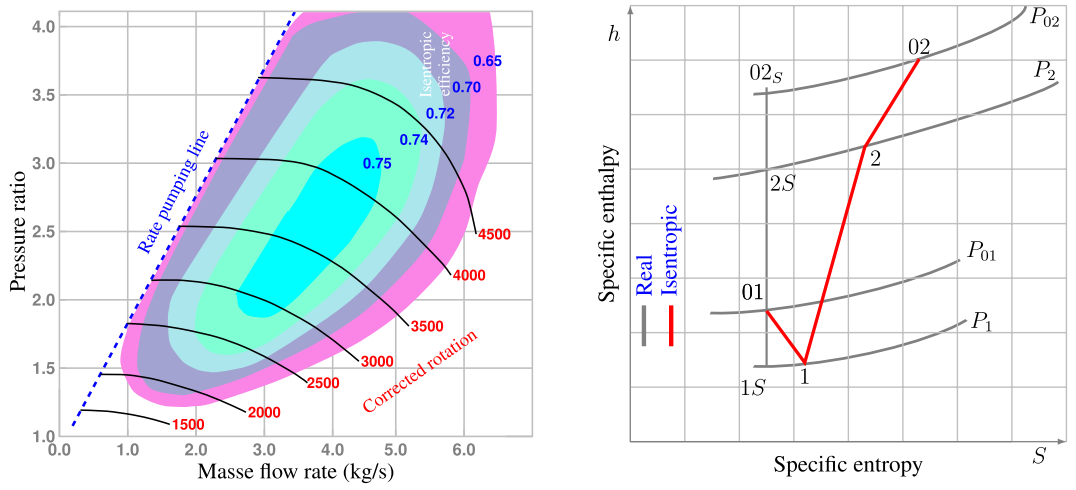

Fig. 4. Field diagram and isentropic efficiency of BCL 505 compressor system.

2.2. The problem of surge phenomenon in centrifugal compressor

In the operation of a compressor, a destructive phenomenon occurs that it is imperative to avoid: surge or pumping phenomenon. In principle, the compressor connected to two networks at different pressures, aspiration (low-pressure) and discharge (high-pressure). The pumping occurs when the high-pressure network of the discharge empties into the low-pressure network of aspiration by a flow against the flow in the compressor. This phenomenon, which can have several causes, provokes momentary instability of the ventilation network (a case where the gas is air). When the discharge network has emptied itself sufficiently in the aspiration, the compressor finds operating conditions allowing it to restore flow to the correct direction, until a new cycle of instability begins again. These large flow fluctuations are therefore called pumping, due to the oscillatory nature of the back-and-forth phenomenon of the flow. Possible causes of surge phenomena in a centrifugal compressor: Reduction in the density of the gas, due to a change in the molecular weight of its composition. Increase in temperature of aspiration T1 at the inlet. Reduction of the rotation speed. If the new rotation speed applied on the compressor cannot produce the required pressure by the industrial process. Blockage of any flow chain, aspiration or discharge. Deformation of the wheel geometry, by erosion, soiling, etc.

2.3. Problem description

The examined centrifugal compressor system is represented by the uncertain parameters dynamical state-space model as:

$$\begin{cases} \xi_{k+1} = \{A + \Delta A(\theta)\}\xi_k + \{B + \Delta B(\theta)\}\mu_k \\ \mathscr{Y}_k = \{C + \Delta C(\theta)\}\xi_k \end{cases} \quad (1)$$

where

$$\{\Delta A(\theta), \Delta B(\theta), \Delta C(\theta)\} \in \left[\left\{ \underline{A}(\theta), \underline{B}(\theta), \underline{C}(\theta) \right\} \quad \left\{ \overline{A}(\theta), \overline{B}(\theta), \overline{C}(\theta) \right\} \right] \quad (2)$$

θ: is the bounded uncertain matrix parameters of the studied system. $\underline{\bullet}$ and $\overline{\bullet}$ in (2), represent the lower and the upper bound of the uncertain parameters of the studied system matrix, respectively. The numerical model of the studied system (1), which presents all the centrifugal compressor behaviour from the inputs to the outputs, is mentioned in Appendix B. Fig. 5 and Fig. 6show the real outputs of the discharge pressure and temperature respectively, it appears clearly through the two curves of the outputs, the symptoms of the surge phenomenon, the

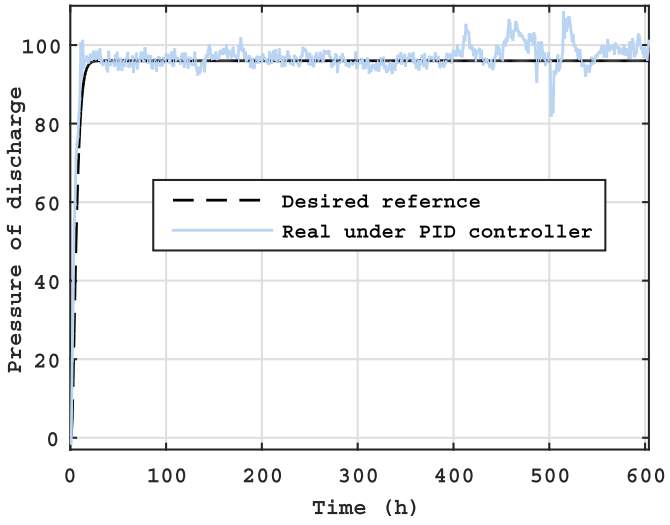

Fig. 5. The required and the measured discharge pressure P2.

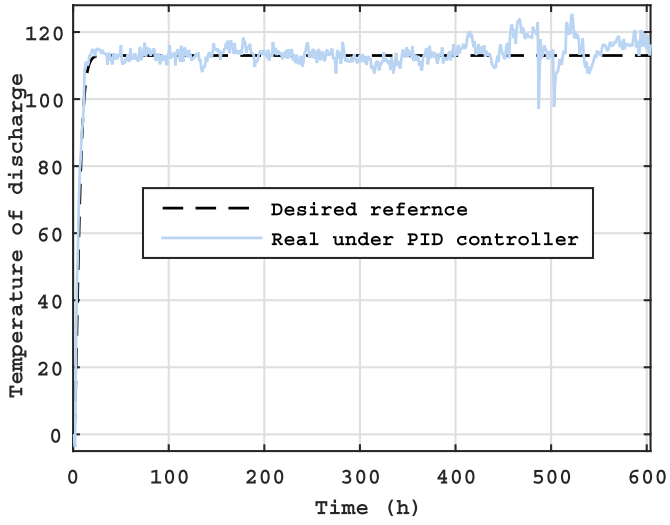

Fig. 6. The required and the measured discharge temperature T2.

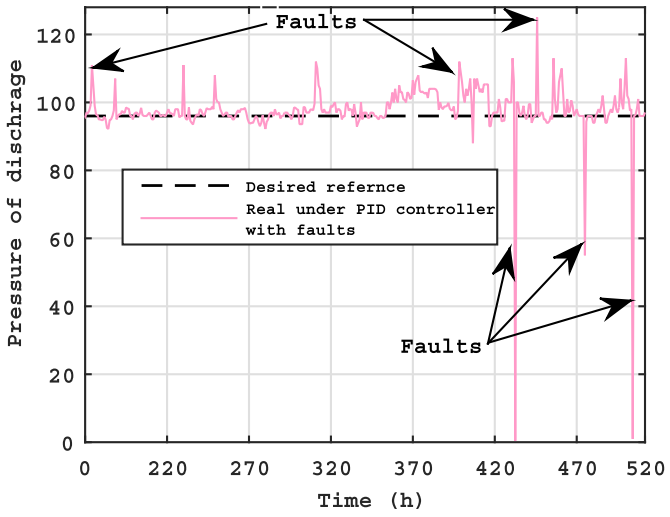

Fig. 7. Faulty discharge pressure P2 signal with faults.

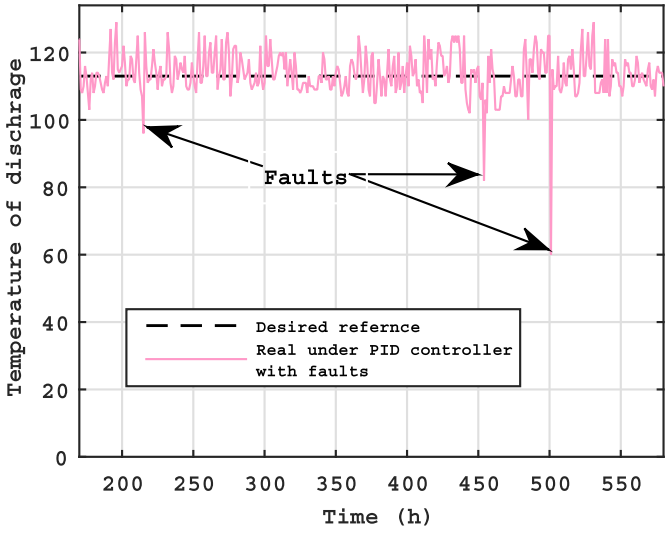

Fig. 8. Faulty discharge temperature T2 with faults.

measured discharge pressure and temperature not coincide to its required references, an irregular flow, with fluctuations, oscillations and peaks in the outputs.

The system continued to operate in the presence of the above symptoms of the surge phenomenon (degraded mode). The previous symptoms began to develop into danger defects as appear in Fig. 7 and Fig. 8, aggravation in the flow oscillations of the measured outputs, and the appearance of peaks with significant amplitude (faults). Real photos of the studied system BCL 505 gas compressor in schedule revision. Fig. 9 shows scratches on the blades of the impeller one and light streaks at the spacers, and Fig. 10 shows damage in o-ring joints. We examine the robustness of internal stability of the studied dynamical model against the uncertainties in the parameters by adding Δ to the nominal model as in (6). Where $\Delta = [+0\%, +10\%, +20\%, +30\%, +40\%, +50\%]$ and checking the internal stability in each value of interval Δ. Based on Fig. 11 the studied system remains internally stable in the interval uncertainties of $\Delta = [+0\%, +10\%, +20\%]$, where all poles located inside the unit circle. The system loses its internal stability if the added uncertainties $\Delta \geq +30\%$, where some poles outside the unit circle.

The description of the BCL 505 centrifugal compressor system behaviour by presenting in detail the influence of the surge phenomenon to its thermodynamic parameters, proved the inability of conventional industrial PID controller embedded in the system of the DCS, to eliminate the surge phenomenon, and to maintain the flow of the real measurement of the discharge P2 and T2 in the level of the desired references, and to control susceptible system to the added uncertainties, with fragility in its internal stability. In this regard, we suggest supporting the embedded industrial PID controller by a new optimal output feedback controller K to help reduce the surge phenomenon and improve the internal stability of the compressor against the uncertainties of the parameters as shown in Fig. 12.

Applying feedback controller $\mu_k = -K\mathscr{Y}_k$ as shown in Fig. 12, (1) can be rewritten as follows:

$$\begin{cases} \xi_{k+1} = \{A + \Delta A(\theta)\}\xi_k - \{B + \Delta B(\theta)\}K\mathscr{Y}_k \\ \mathscr{Y}_k = \{C + \Delta C(\theta)\}\xi_k \end{cases} \tag{3}$$

(3) can be again expressed as:

$$\begin{cases} \xi_{k+1} = \left(\underbrace{\{A + \Delta A(\theta)\} - \{B + \Delta B(\theta)\}K\{C + \Delta C(\theta)\}}_{\mathscr{F}(\theta)} \right)\xi_k \\ \mathscr{Y}_k = \{C + \Delta C(\theta)\}\xi_k \end{cases} \tag{4}$$

where $\mathscr{F}(\theta)$ is the feedback matrix of the CLS. In the next section, we introduce the proposed algorithm that finds the output static feedback matrix K.

3. Main results of the proposed algorithm

Usually, the output feedback controller is influenced by both $\{B+\Delta B(\theta)\}$ and $\{C+\Delta C(\theta)\}$ matrices from the right and left respectively, which allows using CBT characteristic, which is the foremost idea in the proposed controller design. $\mathscr{F}(\theta)$ in (4) can be expressed as:

$$\{B + \Delta B(\theta)\}K\{C + \Delta C(\theta)\} = \{A + \Delta A(\theta)\} - \mathscr{F}(\theta) \tag{5}$$

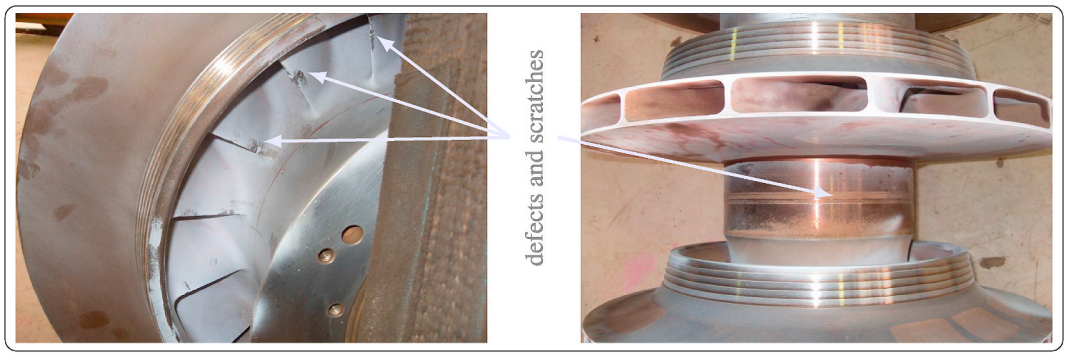

Fig. 9. BCL 505 centrifugal compressor in scheduled revision (defects and scratches).

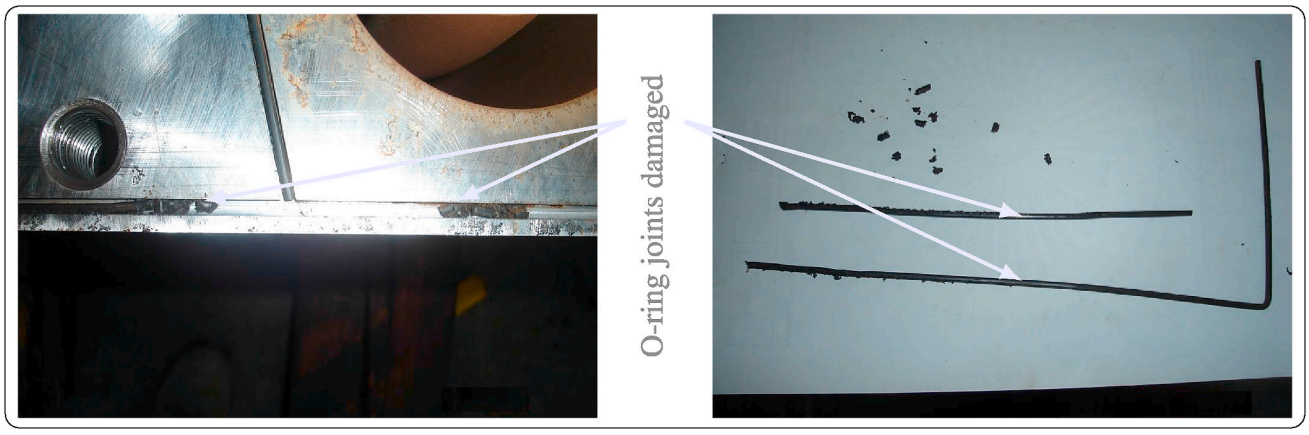

Fig. 10. BCL 505 centrifugal compressor in scheduled revision (O-ring joints damaged).

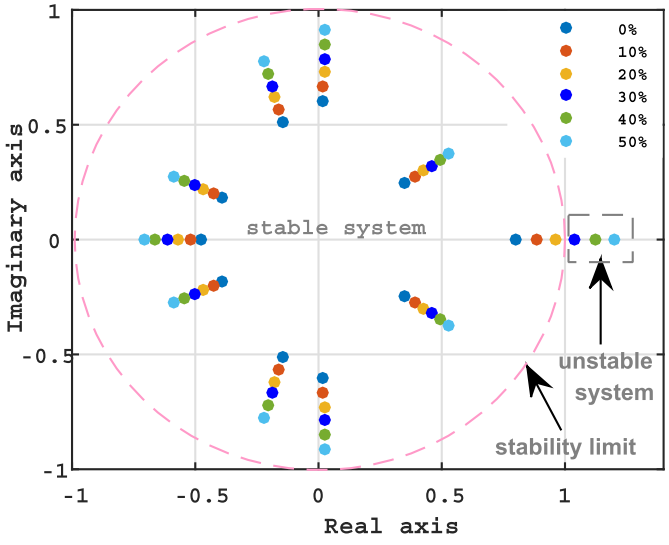

Fig. 11. Internal stability under dynamics uncertainties.

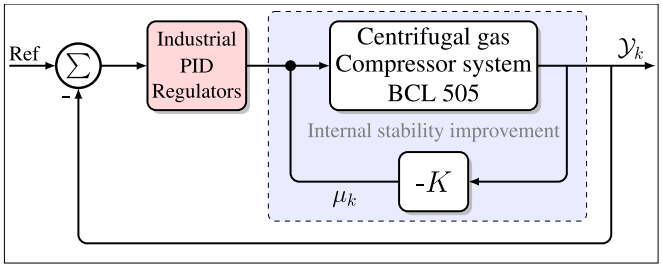

Fig. 12. The proposed scheme of output-feedback controller.

$$A(\theta)_{co} = T_c(\theta)\{A + \Delta A(\theta)\}T_o(\theta) = \begin{pmatrix} \Upsilon_1(\theta) & \Upsilon_2(\theta) \\ \Upsilon_3(\theta) & \Upsilon_4(\theta) \end{pmatrix} \tag{9}$$

where

$$\Upsilon_1(\theta) = A(\theta)_{co}(1:(n-m),1:(n-p)), \Upsilon_2(\theta) = A(\theta)_{co}(1:(n-m),(n-p+1):n)$$

$$\Upsilon_3(\theta) = A(\theta)_{co}((n-m+1):n,1:(n-p)), \Upsilon_4(\theta) = A(\theta)_{co}((n-m+1):n,(n-p+1):n)$$

Multiplying (5) from the left and the right sides by CBT matrix $T_c(\theta)$ and $T_o(\theta)$ respectively as:

$$T_c(\theta)\{B + \Delta B(\theta)\}K\{C + \Delta C(\theta)\}T_o(\theta) = T_c(\theta)(\{A + \Delta A(\theta)\} - \mathscr{F}(\theta))T_o(\theta) \tag{6}$$

Based on definitions of $T_c(\theta), T_o(\theta), B_c(\theta), C_o(\theta)$ [see Appendix B] we get:

$$\begin{pmatrix} Z_m & Z_m & \cdots & Z_m \\ Z_m & Z_m & \vdots & Z_m \\ \vdots & \ddots & \vdots & \vdots \\ Z_m & Z_m & \cdots & K \end{pmatrix} = T_c(\theta)(\{A + \Delta A(\theta)\} - \mathscr{F}(\theta))T_o(\theta) \tag{7}$$

By putting $T_c(\theta)(\{A + \Delta A(\theta)\} - \mathscr{F}(\theta))T_o(\theta) = \Lambda(\theta)_{co}$, $\Lambda(\theta)_{co} \in \mathbb{R}^{n\times n}$, and from it, K is extracted as follows:

$$K = \Lambda(\theta)_{co}((n-m+1):n,(n-p+1):n) \tag{8}$$

The matrix $\mathscr{F}(\theta)$ must achieve desired performance to be determined as:

Based on (7), (9), $T_c(\theta)$, $T_o(\theta)$, $\Upsilon_1(\theta)$, $\Upsilon_2(\theta)$, $\Upsilon_3(\theta)$ and $\Upsilon_4(\theta)$, the desired matrix $\mathscr{F}(\theta)$ is parameterized as:

$$T_c(\theta)\mathscr{F}(\theta)T_o(\theta) = \begin{pmatrix} \Upsilon_1(\theta) & \Upsilon_2(\theta) \\ \Upsilon_3(\theta) & \Upsilon_4(\theta) \end{pmatrix} - \begin{pmatrix} Z_m & Z_m & \cdots & Z_m \\ Z_m & Z_m & \vdots & Z_m \\ \vdots & \ddots & \vdots & \vdots \\ Z_m & Z_m & \cdots & K \end{pmatrix} \tag{10}$$

and

$$\mathscr{F}(\theta) = T_c(\theta)^{-1}\begin{pmatrix} \Upsilon_1(\theta) & \Upsilon_2(\theta) \\ \Upsilon_3(\theta) & \Upsilon_4(\theta) - K \end{pmatrix}T_o(\theta)^{-1} \tag{11}$$

Remark 1. $T_c(\theta)$ and $T_o(\theta)$ assumed to be nonsingular.

Finally,

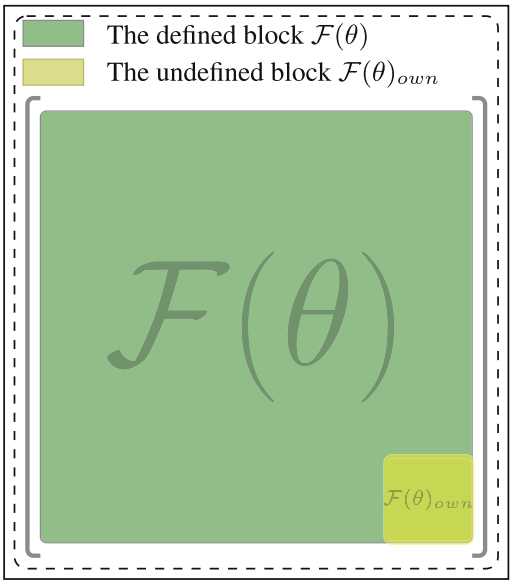

Fig. 13. Scheme of feedback matrix.$\mathscr{F}(\theta)$

$$\Lambda_{co}(\theta) = \begin{pmatrix} Z_m & Z_m & \cdots & Z_m \\ Z_m & Z_m & \vdots & Z_m \\ \vdots & \ddots & \vdots & \vdots \\ Z_m & Z_m & \cdots & K \end{pmatrix} \equiv K = \Upsilon_4(\theta) - \mathscr{F}_{own}(\theta) \tag{12}$$

K, $\Upsilon_4(\theta)$ and $\mathscr{F}_{own}(\theta) \in \mathbb{R}^{m\times p}$ The block own matrix $\mathscr{F}_{own}(\theta)$ describes the specification of the CLS. Furthermore, it holds the full set information about the internal stability of the feedback matrix $\mathscr{F}(\theta)$, which it decides on the convergence of compressor system behaviour in the spectrum eigenspace from the input to the output. Fig. 13 describes the ratio between the defined block of the feedback matrix $\mathscr{F}(\theta)$ and the undefined one which is the block own matrix $\mathscr{F}_{own}(\theta)$. The impact of the CBT used in the proposed design is adequately clear, where it compresses the undefined desired dynamic to a little matrix $\mathscr{F}_{own}(\theta)$ in the corner of the global feedback matrix $\mathscr{F}(\theta)$. Therefore, the computing of the own matrix $\mathscr{F}_{own}(\theta)$, allows defining all the elements of the desired feedback matrix $\mathscr{F}(\theta) \in \mathbb{R}^{n\times n}$, as shown in Fig. 15.

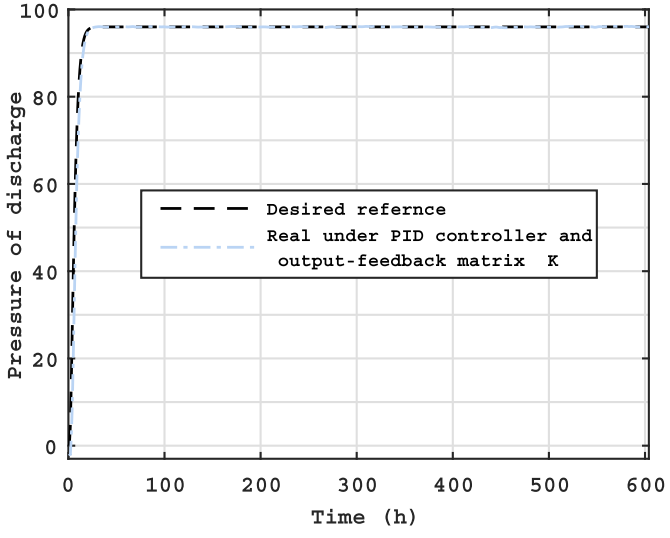

Fig. 14. The measured discharge pressure P2 under output-feedback controller K.

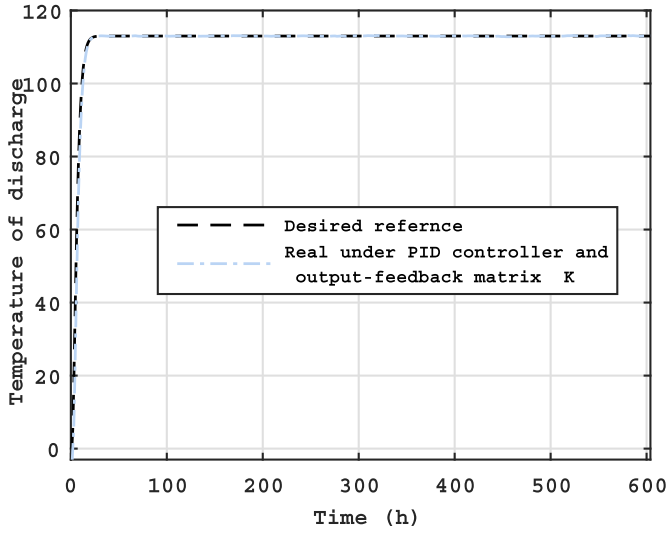

Fig. 15. The measured discharge temperature T2 under output-feedback controller K.

3.1. How to choice the block own matrix $F_{own}(\theta)$

The use of pole assignment method to design the output-feedback matrix gain is insignificant, where the space dimension of the controller gain is inadequate, i.e. $\dim(K) \leq \dim(A(\theta))$, therefore the desired internal stable poles, not all have an image in the space of the controller (Nail et al., 2016). Thus, the choice of poles internally stable is involved in this case. In this work, the block own matrix $\mathscr{F}_{own}(\theta)$ is considered a convex problem and formulating to an optimization objective function $f(\mathbf{x})$ with constraints and solved by GWO. The GWO is a meta-heuristic optimizer proposed by Mirjalili et al. (2014), chosen as a tool to solve the convex optimization problems, its selection from various evolutionary and meta-heuristics methods, based on its quick convergence and simple tuning (Mirjalili et al., 2014). The objective function $f(\mathbf{x})$ is chosen as:

$$f(\mathbf{x}) = K(\mathbf{x})_\infty = \Upsilon_4(\theta) - \mathscr{F}_{own}(\mathbf{x})_\infty \tag{13}$$

Find $\mathbf{x}$ of own block matrix $\mathscr{F}_{own}(\mathbf{x})$ which minimizes $K(\mathbf{x})_\infty$, subject to the following constraints:

$$\begin{aligned} &|\text{eigenvalues}(\mathscr{F}(\theta))| - \varepsilon < 0, \qquad \varepsilon \in]01[, \\ &\text{lower bound} \leq \mathbf{x}_k \leq \text{upper bound}, \qquad k = \overline{1,\ldots,m\times p} \end{aligned} \tag{14}$$

The best choice of the inequality constraint condition assures the internal stability of the feedback matrix $\mathscr{F}(\theta)$, which oblige the eigenvalues located inside the unit circle. The interval of the lower and the

Table 1
Comparison study: in internal stability and norm.

Algorithm	K	Norm of K	Internal stability
GWO	$\begin{pmatrix} -0.1881 & -0.2351 \\ -0.0419 & 0.6566 \end{pmatrix}$	0.69	[0.26, 0.60]
GA	$\begin{pmatrix} 0.5761 & -0.4052 \\ -0.5179 & 1.1118 \end{pmatrix}$	1.37	[0.39, 0.96]
PSO	$\begin{pmatrix} -1.2452 & -0.2846 \\ 0.3177 & 1.0178 \end{pmatrix}$	1.45	[0.37, 0.99]
IPM	$\begin{pmatrix} 1.4358 & 0.1793 \\ -0.8239 & 0.6081 \end{pmatrix}$	1.66	[0.61, ~1]
Algorithm (Řezáč and Hurák, 2013)	$\begin{pmatrix} -1.8155 & -0.5717 \\ 0.6240 & 1.1656 \end{pmatrix}$	2.17	[0.37, 0.98]
Algorithm (Veselý, 2001)	$\begin{pmatrix} -1.0684 & -1.0548 \\ 0.4757 & 1.5049 \end{pmatrix}$	2.11	[0.48, 0.98]

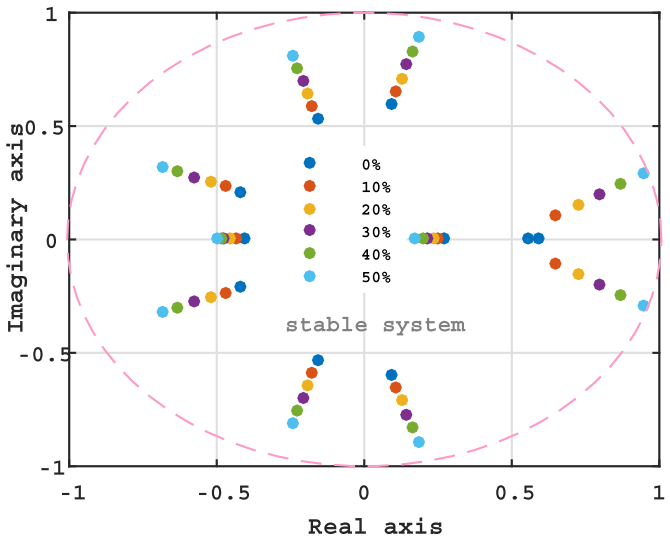

Fig. 16. Internal stability under output-feedback controller K.

upper bound optimization vector $\mathbf{x}_k$ chosen near to the value of the matrix Υ_4.The proposed controller summarized in the following steps:

3.2. The proposed algorithm

Step1. Calculate CBT matrix $T_c(\theta)$ and $T_o(\theta)$ as in (17) and (19), see Appendix B.

Step2. Calculate the matrix $\Lambda_{co}(\theta)$, as (8).

Step3. Extract the matrix $\Upsilon_4(\theta)$ from $\Lambda_{co}(\theta)$, as (9).

Step4. Compute the feedback matrix controller K based on GWO, as: (a).

- Determine the own block matrix $\mathcal{F}_{own}(\mathbf{x})$, which fit the minimum norm of output-feedback controller K as in (13).
- Check the feasibility of the internal stability constraints as in (14).

Step5. Finally, After fulfilling the specified number of the iteration, the best block own matrix $\mathcal{F}_{own}(\mathbf{x})$ was elected, with optimal output-feedback matrix gain K as in (12).

4. Application and results discussion

To achieve the principal objectives of this paper, the proposed algorithm executed on the studied compressor system, by following steps

Table 2
Comparison study: in time specifications.

U	Y	Time speciffcations	Algorithm (Řezák and Hurák, 2013)	Algorithm (Veselý, 2001)	Proposed Algorithm
90From aspiration temperature T1	90To discharge pressure P2	$\mathbf{t_r}$	172	159	4
		$\mathbf{t_p}$	479	519	7
		Peak	185.6374	79.6770	0.3821
		$\mathbf{U_{shoot}}$	0.4381	1.6783	0
		$\mathbf{O_{shoot}}$	0	0	0.2641
		$\mathbf{S_{Max}}$	−167.4240	−71.7362	0.3821
		$\mathbf{S_{Min}}$	−185.6374	−79.6770	0.3645
		$\mathbf{t_s}$	306	284	6
	90To discharge temperature T2	$\mathbf{t_r}$	173	161	5
		$\mathbf{t_p}$	479	519	69
		Peak	654.5301	709.8274	0.7881
		$\mathbf{U_{shoot}}$	0.0122	0.0113	10.1520
		$\mathbf{O_{shoot}}$	0	0	0
		$\mathbf{S_{Max}}$	654.5301	709.8274	0.7881
		$\mathbf{S_{Min}}$	590.5383	639.7949	0.7118
		$\mathbf{t_s}$	301	275	11
90From aspiration pressure P1	90To discharge pressure P2	$\mathbf{t_r}$	172	159	4
		$\mathbf{t_p}$	479	519	11
		Peak	295.2633	144.7808	0.7182
		$\mathbf{U_{shoot}}$	0.5964	1.9586	0
		$\mathbf{O_{shoot}}$	0	0	0.0838
		$\mathbf{S_{Max}}$	−266.2478	−130.5518	0.7182
		$\mathbf{S_{Min}}$	−295.2633	−144.7808	0.6721
		$\mathbf{t_s}$	307	285	7
	90To discharge temperature T2	$\mathbf{t_r}$	173	161	6
		$\mathbf{t_p}$	479	519	69
		Peak	$1.0428 \times 10^{+3}$	$1.2938 \times 10^{+3}$	0.8008
		$\mathbf{U_{shoot}}$	0.0040	0.0032	5.1504
		$\mathbf{O_{shoot}}$	0	0	0
		$\mathbf{S_{Max}}$	$1.0428 \times 10^{+3}$	$1.2938 \times 10^{+3}$	0.8008
		$\mathbf{S_{Min}}$	940.8059	$1.1661 \times 10^{+3}$	0.7255
		$\mathbf{t_s}$	302	276	12

Table 3

The eigenvalues sensitivity of compressor system.

$s(\lambda_{i=1..10})$	1	2	3	4	5	6	7	8	9	10
Proposed algorithm	26.2867	32.8166	14.5680	3.4064	3.4064	4.6529	4.5529	4.0717	1.2853	5.2853
Algorithm (Řezáč and Hurák, 2013)	35.1612	48.9137	23.5602	4.2572	4.2572	12.3833	4.5859	4.5859	2.1985	2.1985
Algorithm (Veselý, 2001)	3.9905	3.9905	42.4162	60.9825	5.4663	5.4663	20.0368	32.7376	2.2328	2.2328

Table 4

The Relative change in the eigenvalues of compressor system.

$r(\lambda_{i=1..10})$	1	2	3	4	5	6	7	8	9	10
Proposed algorithm	0.0341	0.0260	0.0104	0.0029	0.0029	0.0047	0.0047	0.0046	0.0046	0.0046
Algorithm (Řezáč and Hurák, 2013)	0.0463	0.0407	0.0145	0.0037	0.0037	0.0072	0.0049	0.0049	0.0049	0.0049
Algorithm (Veselý, 2001)	0.0035	0.0035	0.0518	0.0477	0.0049	0.0049	0.0123	0.0192	0.0050	0.0050

Table 5

Stability measures of compressor system.

1 pt]1–4 Algorithms	Measure1	Measure2	Measure3
Proposed algorithm	0.0171	0.0012	0.0276
Algorithm (Řezáč and Hurák, 2013)	0.0196	0.0033	0.0192
Algorithm (Veselý, 2001)	0.0204	0.0019	0.0147

as mentioned earlier as follows:

1. Calculate CBT matrices $\{T_c(\theta), T_o(\theta)\}$ and their numerical values mentioned in Appendix B, (21) and (22).
2. Calculate $\Lambda_{co}(\theta)$ its numerical value mentioned in Appendix B, see (23).
3. Extracte $\Upsilon_4(\theta) \in R^{2\times 2}$ from $\Lambda_{co}(\theta)$, its value given as: $\Upsilon_4 = \begin{pmatrix} -3.6760 & -1.8422 \\ 2.5662 & 2.0853 \end{pmatrix}$
4. Compute the output-feedback controller matrix gains K based on minimizing the objective function $||K||_\infty$ using GWO subject to: $|\text{eigenvalues}(\mathscr{F}(\theta))| - 0.6 < 0$, thus the internal stability is ensured, i. e the poles inside the unit circle. The lower and the upper bound of the optimization vector chosen as $\mathbf{x} \in [-1010]$, where $\mathbf{x} \in \mathbb{R}^{1\times 4}$. This interval presents the search space as shown in Fig. 17. The number of iterations = 400, and the search agents number = 20, as shown in Fig. 17.
5. The best own block matrix given as: $\mathscr{F}_{own}(\mathbf{x}) = \begin{pmatrix} -3.4879 & -1.6071 \\ 2.6081 & 1.4287 \end{pmatrix}$ The output-feedback controller matrix gains K is chosen optimally as: $K = \begin{pmatrix} -0.1881 & -0.2351 \\ -0.0419 & 0.6566 \end{pmatrix}$

The obtained results proved the effectiveness of the proposed output-feedback controller K through eliminating the surge phenomenon, where the flow-oscillations and the peaks disappeared from the two outputs parameters, as shown in Fig. 14 and Fig. 15fig19, respectively. Furthermore, its influence on internal stability robustness, where the compressor system remained to maintain its internal stability under 50% of parameters uncertainties, as shown in Fig. 16. Where the eigenvalues of the compressor located inside the unit circle in the region of convergence.

4.1. Comparative study

In Table 1, two comparative studies are introduced to illustrate the added value of the proposed controller vs the approaches existed in literature. The first comparative study demonstrates the effectiveness of GWO algorithm to estimate the elements of the own block matrix compared by popular methods: evolutionary GA (Chehouri et al., 2016), swarm PSO (Mazhoud et al., 2013) and linear programming IPM (Waltz et al., 2006), respectively. The second comparative study demonstrates the reliability of CBT similarity on the proposed design compared by two controllers designed based on H_∞ and Lyapunov theory. The GWO gives a useful optimization in the norm of output-feedback controller gains K, and in the interval of internal stability, where provides a suppleness to locate any desired eigenvalues in any region inside the unit circle. Furthermore, in the second comparative study with two robust controllers, the obtained results show an advantage in the norm of K **0.69**, which means internal stability in CLS guaranteed with the most economical energy.

Table 2 shows the specifications time of feedback compressor system: Peak time ($\mathbf{t_p}$)), Peak (**Peak**), Undershoot ($\mathbf{U_{shoot}}$), Overshoot ($\mathbf{O_{shoot}}$), Settling max ($\mathbf{S_{Max}}$), Settling min ($\mathbf{S_{Min}}$), Settling time ($\mathbf{t_s}$), and Rise time ($\mathbf{t_r}$). Based on the assessment of results shown in Table 2, the proposed controller achieves the desired specification time in the majority of response characteristics, except in some undershoot and overshoot component, which permits the compressor system to maintain their achievements under uncertainty and in the effect of surge phenomenon.

Table 3 exhibits the sensitivity of eigenvalues in the presence of uncertainties in the studied compressor system. It is obvious the proposed controller perform robustness stability vs the compared algorithms, which explains the internal durability of the compressor system dynamics (Nail et al., 2019) and (Tsui, 1994).

Table 4 and Table 5 are present the relative change in eigenvalues and the stability measures of the studied compressor system, respectively. The results show a minimum variation in the changed

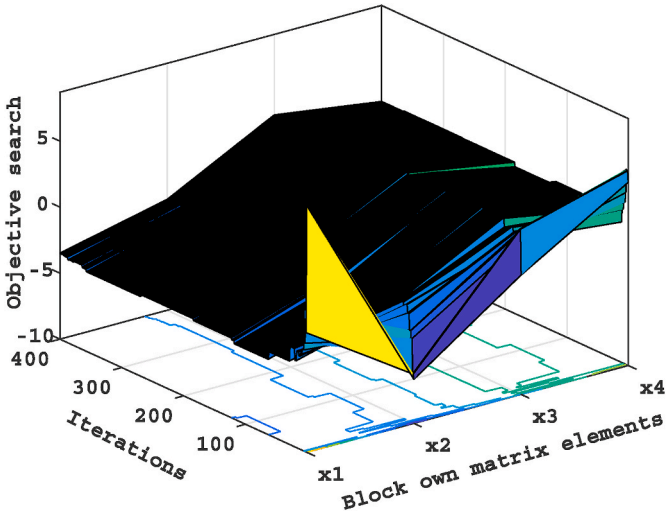

Fig. 17. Selection of block own matrix elements using GWO.

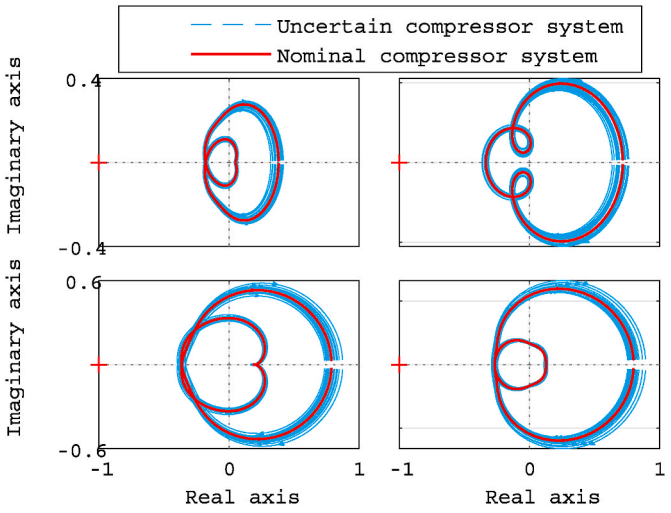

Fig. 18. Nyquist plot of the compressor system.

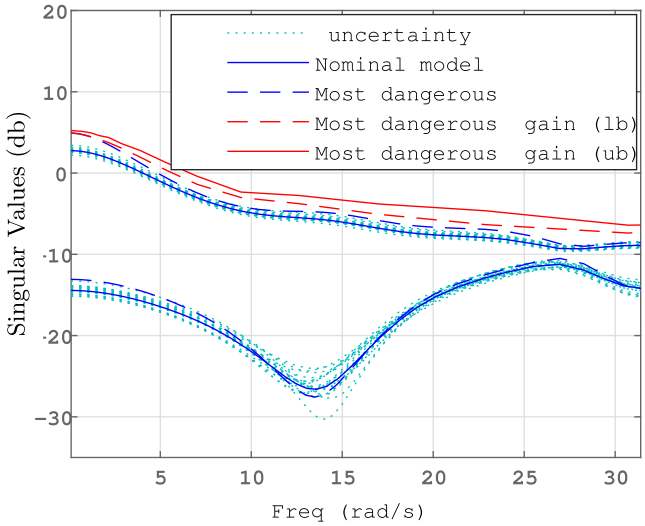

Fig. 20. Most dangerous gain of the compressor system.

eigenvalues of the compressor system and a significant difference in the compared algorithms, which make internal stability problem. Furthermore, based on the definition of the three stability measurements (Nail et al., 2019) and (Tsui, 1994), the proposed controller satisfies the requirements of the most suitable stability measurements.

4.2. *Frequency analysis*

In this subsection, the frequency analysis of the studied compressor system under some conditions carried out. Fig. 18 explains the Nyquist diagram, where the stability defined by examining how Nyquist contour mapped by the uncertain model of the compressor system, we find the system in open loop is stable. The internal stability of the compressor system ensured via Nyquist diagram because the map not enclose the critical-point $(-1,0)$ as shown in Fig. 18. Fig. 19 gives the robust boundary stability for the uncertain parameters compressor model, we see that the boundary stability dependent to the level uncertainty in model parameter defined as $\Delta\theta \in [-50\% + 50\%]$, the interval in the curve with blue colour is higher than one > 1 in each point in frequency axis from 0 to 100 (rad/s), which indicates that the compressor system is internally stable for any values of uncertainty. Excluding when the interval is smaller than one < 1, a critical point appears of coordinate (71 rad/s) in frequency axis and boundary stability $= (0.9057)$. This point indicates that the compressor system becomes internally unstable due to the interval areas include some values of uncertain model parameters. However, the critical point not affected the general internal stability of the compressor system. Fig. 20 gives the nominal and most dangerous cases gains of the uncertain compressor system, where the gains lead to the most significant singular value of the response frequency. Therefore after when the uncertainties involved on the compressor system, no substantial change in the most considerable singular value $\overline{\sigma}$. Fig. 21 exhibits the singular values frequency analysis of the uncertain feedback compressor system, where it is useful for robustness study, within the curve no critical variation for the highest singular value $\overline{\sigma}$.

5. Conclusion

This paper focused on improving the set-point regulation of two outputs thermodynamic parameters: the discharge compressor and temperature, respectively in the BCL 505 centrifugal compressor system where the sharpness of the surge phenomenon has eliminated, via enhancing the internal dynamic stability of the studied system. The gains mentioned above have been achieved by the proposed output-feedback controller matrix K. Furthermore contributed to the normal-

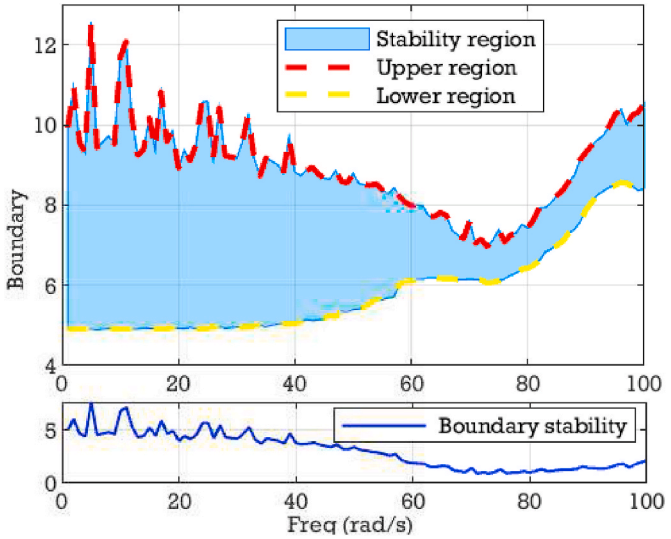

Fig. 19. Robust stability of the compressor system.

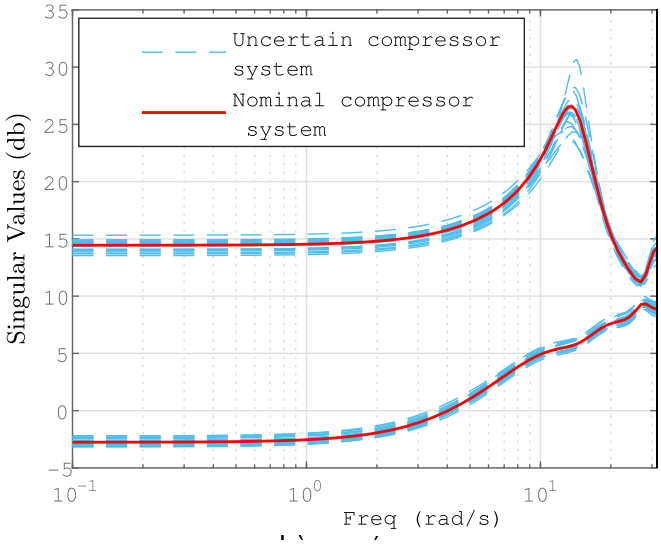

Fig. 21. Singular values of the compressor system.

mode operation of the studied system and maintained the pressure of the natural gas according to the demand that the consumer wants. The dangers peaks, the undesirable fluctuations and oscillations, have eliminated, where some of them reach the height of $\pm$ 21.63 kg/cm^2 in discharge pressure and $\pm$7.27 $^\circ$C in discharge, compared with their set-points outputs P2 $\simeq$ 96 kg/cm and T2 $\simeq$ 113 $^\circ$C, respectively. The stability range [0.26, 0.60] of the compressor system has been extended in the presence of external or internal uncertainties in the parameters or disturbance in the outputs signals, wherein the case of adding 50% uncertainties to the nominal model parameters, the studied system remains stable and usually operates. The proposed controller achieves the desired specification time in the majority of response characteristics, which permits the compressor system to maintain their achievements under uncertainty and in the effect of surge phenomenon. Moreover, we believe that the proposed design is considered a promising contribution which can be generalized to solve many control problems in the industrial field.

The proposed algorithm presents some limitations and constraints with suggested solutions:

- The dynamical model of the system should be parametric in state space representation.
- In the case of the model does not achieve the CBT feature, suggested solutions exist in the literature propose prolonging the space of the system by adding non-governing states to make the system transformable (Shieh et al., 1983).
- Or by eliminating the non-dominate states, i.e. weakly controllable and observable states using model order reduction approaches. Either by our proposition of decoupling the model into block transformable part, and the other part controlled independently using classical pole placement method (Bekhiti et al., 2018).

Authors contribution

Dr. Bachir Nail: Proposed method; Data acquisition; interpretation. Dr. Belkacem Bekhiti: Writing; review & editing; Software. Pr. Vicenç Puig: Supervision in the internship; Validation; mathematics and theory revision.

Declaration of competing interest

The authors declare that they have no known competing financial interests or personal relationships that could have appeared to influence the work reported in this paper.

Acknowledgements

The authors are grateful to the editor, the supervisor editor, the executive editor and the anonymous referees for their constructive comments and valuable suggestions which improved the quality of the paper, and to all staff of Hassi R'Mel natural gas field, Laghouat, Algeria

Appendix A

Table 6
BCL 505 centrifugal gas compressor characteristics

Parameter	Value
Stages of compressor	1–5
Pressure of discharge (Max)	123 kg/cm^2
Temperature of discharge (Max)	121 $^\circ$C
Efficiently %	73%
Rotor speed	3000–20000 rpm
Type of gas	LNG

Appendix B

In this appendix we introduce preliminaries on block canonical form transformation (CBT) which consider basic tools for constructing the proposed controller (Shieh et al., 1983), (Bekhiti et al., 2018) and (Yaici and Hariche, 2014). In the following the state space representation of a linear multivariable discrete-time system:

$$\begin{cases} \xi_{k+1} = A\xi_k + B\mu_k \\ \mathscr{Y}_k = C\xi_k + D\mu_k \end{cases} \tag{15}$$

$\xi \in \mathbb{R}^n$ is the general state variable vector, $A \in \mathbb{R}^{n\times n}$ is the system matrix, $B \in \mathbb{R}^{n\times m}$ is the control matrix, $C \in \mathbb{R}^{p\times n}$ is the output matrix and $D \in \mathbb{R}^{p\times m}$ is the coupling matrix. The controllability space χ_c is generated by the vectors A^iB as

$$\chi_c = \operatorname{span}\left\{A^iB\right\}_{i=i+1} \Leftrightarrow \Omega_c = \operatorname{row}\left(A^iB\right)_{i=0}^{l-1} \tag{16}$$

where Ω_c is called the block controllability matrix.

$$\begin{cases} \xi_{c(k+1)} = \left\{A_c = T_cAT_c^{-1}\right\}\xi_{ck} + \{B_c = T_cB\}\mu_k \\ \mathscr{Y}_k = \left\{C_c = CT_c^{-1}\right\}\xi_{ck} + \{D_c = D\}\mu_k \end{cases} \text{with} \left\{T_c = \operatorname{col}\left\{T_{c1}A^i\right\}_{i=0}^{l-1}T_{c1} = B_c^T\left(\operatorname{row}\left(A^iB\right)_{i=0}^{l-1}\right)^{-1}\right. \tag{17}$$

The observability space χ_o is generated by the vectors CA^i as

$$\chi_o = \operatorname{span}\left\{CA^i\right\}_{i=i+1} \Leftrightarrow \Omega_o = \operatorname{row}\left(CA^i\right)_{i=0}^{l-1} \tag{18}$$

where Ω_o is called the block observability matrix.

$$\begin{cases} \xi_{o(k+1)} = \{A_o = T_o^{-1} A T_o\}\xi_{ok} + \{B_o = T_o^{-1} B\}\mu_k \\ \mathscr{Y}_k = \{C_o = C T_o\}\xi_{ok} + \{D_o = D\}\mu_k \end{cases} \text{with} \left\{ T_o = \text{row}\left\{A^i T_{o1}\right\}_{i=0}^{l-1} T_{o1} = \left(\text{col}\left(CA^i\right)_{i=0}^{l-1}\right)^{-1} C_o^T \right. \tag{19}$$

I_m, I_p and O_m, O_p represent the identity and the zero matrices respectively, and T denotes the transpose. μ_k is the input variable vector (Forcing function) and $\mathscr{Y}_k$ is the output variable vector (measurement function). ξ_{ck} is the controllability state variable vector and ξ_{ok} is the observability state variable vector. **row** stands for the block row operator, **col** stands for the block column operator and **span** stands for the generation of maximum linearly independent vectors.

Remark 2.

The System (15) is block canonical transformable into both controllable and observable forms respectively, if rank of $\{\Omega_c, \Omega_o\} = n$, and the ratio $\{n/m, n/p\} = l$ is integer.

$$A = \begin{pmatrix} 0 & 0 & 0 & 0 & 0 & 0 & 0 & 0 & -0.0152 & 0.0185 \\ 0 & 0 & 0 & 0 & 0 & 0 & 0 & 0 & 0.0389 & 0.0436 \\ 1 & 0 & 0 & 0 & 0 & 0 & 0 & 0 & 0.0666 & 0.0696 \\ 0 & 1 & 0 & 0 & 0 & 0 & 0 & 0 & 0.0881 & 0.1080 \\ 0 & 0 & 1 & 0 & 0 & 0 & 0 & 0 & 0.0959 & 0.0784 \\ 0 & 0 & 0 & 1 & 0 & 0 & 0 & 0 & 0.0508 & 0.0701 \\ 0 & 0 & 0 & 0 & 1 & 0 & 0 & 0 & -0.0171 & 0.0319 \\ 0 & 0 & 0 & 0 & 0 & 1 & 0 & 0 & 0.1294 & 0.0158 \\ 0 & 0 & 0 & 0 & 0 & 0 & 1 & 0 & -0.0052 & 0.0145 \\ 0 & 0 & 0 & 0 & 0 & 0 & 0 & 1 & 0.0699 & 0.0038 \end{pmatrix} B = \begin{pmatrix} 0.0245 & 0.0262 \\ 0.0686 & 0.0045 \\ 0.0219 & 0.0425 \\ 0.0199 & 0.0710 \\ 0.0820 & 0.2317 \\ 0.1615 & 0.1233 \\ 0.1762 & 0.0941 \\ 0.3274 & 0.1871 \\ 0.0857 & 0.2576 \\ -0.0801 & -0.0413 \end{pmatrix} C^T = \begin{pmatrix} 0 & 0 \\ 0 & 0 \\ 0 & 0 \\ 0 & 0 \\ 0 & 0 \\ 0 & 0 \\ 0 & 0 \\ 0 & 0 \\ 1 & 0 \\ 0 & 1 \end{pmatrix} \tag{20}$$

$$T_c = \begin{pmatrix} -679.4919 & -203.6038 & 405.9417 & -173.2170 & -91.2348 & 121.9159 & -117.3242 & 77.3296 & 56.8379 & -43.1130 \\ 1.4890 & 52.1177 & -488.3920 & 342.0972 & -57.1012 & -76.4414 & 214.3428 & -154.9591 & -37.7518 & 36.9720 \\ 405.9417 & -173.2170 & -91.2348 & 121.9159 & -117.3242 & 77.3296 & 56.8379 & -43.1130 & 20.3015 & -12.3380 \\ -488.3920 & 342.0972 & -57.1012 & -76.4414 & 214.3428 & -154.9591 & -37.7518 & 36.9720 & -53.2351 & 26.8509 \\ -91.2348 & 121.9159 & -117.3242 & 77.3296 & 56.8379 & -43.1130 & 20.3015 & -12.3380 & -23.0780 & 4.3534 \\ -57.1012 & -76.4414 & 214.3428 & -154.9591 & -37.7518 & 36.9720 & -53.2351 & 26.8509 & 30.4522 & -1.6681 \\ -117.3242 & 77.3296 & 56.8379 & -43.1130 & 20.3015 & -12.3380 & -23.0780 & 4.3534 & 6.8652 & 5.3898 \\ 214.3428 & -154.9591 & -37.7518 & 36.9720 & -53.2351 & 26.8509 & 30.4522 & -1.6681 & 887.0922 & -7.4119 \\ 56.8379 & -43.1130 & 20.3015 & -12.3380 & -23.0780 & 4.3534 & 6.8652 & 5.3898 & 7.3954 & 689.5298 \\ -37.7518 & 36.9720 & -53.2351 & 26.8509 & 30.4522 & -1.6681 & 887.0922 & -7.4119 & -13.5382 & -2.8038 \end{pmatrix} \tag{21}$$

$$T_o = \begin{pmatrix} 1 & 0 & 0 & 0 & 0 & 0 & 0 & 0 & 0 & 0 \\ 0 & 1 & 0 & 0 & 0 & 0 & 0 & 0 & 0 & 0 \\ 0 & 0 & 1 & 0 & 0 & 0 & 0 & 0 & 0 & 0 \\ 0 & 0 & 0 & 1 & 0 & 0 & 0 & 0 & 0 & 0 \\ 0 & 0 & 0 & 0 & 1 & 0 & 0 & 0 & 0 & 0 \\ 0 & 0 & 0 & 0 & 0 & 1 & 0 & 0 & 0 & 0 \\ 0 & 0 & 0 & 0 & 0 & 0 & 1 & 0 & 0 & 0 \\ 0 & 0 & 0 & 0 & 0 & 0 & 0 & 1 & 0 & 0 \\ 0 & 0 & 0 & 0 & 0 & 0 & 0 & 0 & 1 & 0 \\ 0 & 0 & 0 & 0 & 0 & 0 & 0 & 0 & 0 & 1 \end{pmatrix} \tag{22}$$

$$\Lambda_{co} = \begin{pmatrix} 405.9417 & -173.2170 & -91.2348 & 121.9159 & -117.3242 & 77.3296 & 56.8379 & -43.1130 & 20.3015 & -12.3380 \\ -488.3920 & 342.0972 & -57.1012 & -76.4414 & 214.3428 & -154.9591 & -37.7518 & 36.9720 & -53.2351 & 26.8509 \\ -91.2348 & 121.9159 & -117.3242 & 77.3296 & 56.8379 & -43.1130 & 20.3015 & -12.3380 & -23.0780 & 4.3534 \\ -57.1012 & -76.4414 & 214.3428 & -154.9591 & -37.7518 & 36.9720 & -53.2351 & 26.8509 & 30.4522 & -1.6681 \\ -117.3242 & 77.3296 & 56.8379 & -43.1130 & 20.3015 & -12.3380 & -23.0780 & 4.3534 & 6.8652 & 5.3898 \\ 214.3428 & -154.9591 & -37.7518 & 36.9720 & -53.2351 & 26.8509 & 30.4522 & -1.6681 & 0.8871 & -7.4119 \\ 56.8379 & -43.1130 & 20.3015 & -12.3380 & -23.0780 & 4.3534 & 6.8652 & 5.3898 & 7.3954 & 0.6895 \\ -37.7518 & 36.9720 & -53.2351 & 26.8509 & 30.4522 & -1.6681 & 0.8871 & -7.4119 & -13.5382 & -2.8038 \\ 20.3015 & -12.3380 & -23.0780 & 4.3534 & 6.8652 & 5.3898 & 7.3954 & 0.6895 & -3.6760 & -1.8422 \\ -53.2351 & 26.8509 & 30.4522 & -1.6681 & 0.8871 & -7.4119 & -13.5382 & -2.8038 & 2.5662 & 2.0853 \end{pmatrix} \tag{23}$$

References

Agney, A., Singh, S., Srinivas, G., 2018. Structural and fluid flow analysis of subsonic aircraft jet engine centrifugal compressor. Mater. Today: *Proceedings* 5 (9), 19507–19516.

Aouaouda, S., Karimi, H.-R., Chadli, M., Jun. 2014. Robust static output-feedback controller design against sensor failure for vehicle dynamics. IET Control Theory & Appl. 8 (9), 728–737.

Bekhiti, B., Dahimene, A., Nail, B., Hariche, K., 2018. On λ-matrices and their applications in MIMO control systems design. Int. J. Model. Ident. Contr. 29 (4), 281–294.

Chehouri, A., Younes, R., Perron, J., Ilinca, A., Jul. 2016. A constraint-handling technique for genetic algorithms using a violation factor. J. Comput. Sci. 12 (7), 350–362.

Chesi, G., Middleton, R.H., Apr. 2018. LMI-based fixed order output feedback synthesis for two-dimensional mixed continuous-discrete-time systems. IEEE Trans. Automat. Contr. 63 (4), 960–972.

Chung, H.-Y., Wu, S.-M., Mar. 2009. Hybrid approaches for regional Takagi-Sugeno static output feedback fuzzy controller design. Expert Syst. Appl. 36 (2), 1720–1730.

Dong, J., Yang, G.-H., Jun. 2013. Robust static output feedback control synthesis for linear continuous systems with polytopic uncertainties. Automatica 49 (6), 1821–1829.

Du, H., Lam, J., Dec. 2006. Energy-to-peak performance controller design for building via static output feedback under consideration of actuator saturation. Comput. Struct. 84 (31), 2277–2290.

Duan, Z., Hao, Y., Jun. 2015. Static output-feedback controller synthesis with restricted frequency domain specifications for time-delay systems. IET Control Theory & Appl. 9 (10), 1608–1614.

Eker, I., Kara, T., Jul. 2003. Operation and control of a water supply system. ISA (Instrum. Soc. Am.) Trans. 42 (3), 461–473.

Estrada-Manzo, V., Lendek, Z., Guerra, T.M., Jan. 2019. An alternative LMI static output feedback control design for discrete-time nonlinear systems represented by Takagi-Sugeno models. ISA (Instrum. Soc. Am.) Trans. 84 (1), 104–110.

Fujimori, A., Jun. 2004. Optimization of static output feedback using substitutive LMI formulation. IEEE Trans. Automat. Contr. 49 (6), 995–999.

Gadewadikar, J., Bhilegaonkar, A., Lewis, F.L., Oct. 2007. Bounded L_2 gain static output feedback: controller design and implementation on an electromechanical system. I*EEE Trans. Ind. Electron.* 54 (5), 2593–2599.

He, Y., Wang, Q.-G., Oct. 2006. An improved ILMI method for static output feedback control with application to multivariable PID control. IEEE Trans. Automat. Contr. 51 (10), 1678–1683.

He, Y., Wu, M., Liu, G.-P., She, J.-H., Nov. 2008. Output feedback stabilization for a discrete-time system with a time-varying delay. IEEE Trans. Automat. Contr. 53 (10), 2372–2377.

Ho Jae Lee and Do Wan Kim, Oct. 2009. Fuzzy static output feedback may Be possible in LMI framework. IEEE Trans. Fuzzy Syst. 17 (5), 1229–1230.

Liu, E., Lv, L., Yi, Y., Xie, P., 2019. Research on the steady operation optimization model of natural gas pipeline considering the combined operation of air coolers and compressors. IEEE Access 7, 83251–83265.

Marjani, A., Baghmolai, A.M., 2016. Analytical and numerical modeling of non-isothermal and steady-state gas transportation network and the comparison with the results of artificial neural network(ANN) and fuzzy inference system (FIS). J. Nat. Gas Sci. Eng. 36 (11), 1–12.

Mazhoud, I., Hadj-Hamou, K., Bigeon, J., Joyeux, P., Apr. 2013. Particle swarm optimization for solving engineering problems: a new constraint-handling mechanism. Eng. Appl. Artif. Intell. 26 (4), 1263–1273.

Meroni, A., Zühlsdorf, B., Elmegaard, B., Haglind, F., Dec. 2018. Design of centrifugal compressors for heat pump systems. Appl. Energy 232, 139–156.

Mirjalili, S., Mirjalili, S.M., Lewis, A., Mar. 2014. Grey wolf optimizer. Adv. Eng. Software 69, 46–61.

Nail, B., Kouzou, A., Hafaifa, A., Bekhiti, B., 2016. Parametric output feedback stabilization in MIMO systems: application to gas turbine power plant. In: 2016 8th International Conference on Modelling, Identification and Control (ICMIC), Algiers, Algeria, pp. 971–976.

Nail, B., Kouzou, A., Hafaifa, A., Chaibet, A., Jun. 2018. Parametric identification and stabilization of turbo-compressor plant based on matrix fraction description using experimental data. J. Eng. Sci. Technol. 13 (6), 1850–1868.

Nail, B., Kouzou, A., Hafaifa, A., May. 2019. Robust block roots assignment in linear discrete-time sliding mode control for a class of multivariable system: gas turbine power plant application. Trans. Inst. Meas. Contr. 41 (5), 1216â€–1232.

Nail, Bachir, Abdellah, Kouzou, Ahmed, Hafaifa, Hadroug, Nadji, Puig, Vicenç, May. 2019. A Robust fault diagnosis and forecasting approach based on Kalman filter and Interval Type-2 Fuzzy Logic for efficiency improvement of centrifugal gas compressor system. Diagnostyka 20 (2), 57–75.

Nguyen, A.-T., Chevrel, P., Claveau, F., Mar. 2018. Gain-scheduled static output feedback control for saturated LPV systems with bounded parameter variations. Automatica 89, 420–424.

Niknam, P.H., Mortaheb, H.R., Mokhtarani, B., 2018. Dehydration of low-pressure gas using supersonic separation: experimental investigation and CFD analysis. J. Nat. Gas Sci. Eng. 52 (4), 202–214.

Palacios-Quiñonero, F., Rubió-Massegú, J., Rossell, J.M., Karimi, H.R., Jan. 2014a. Feasibility issues in static output-feedback controller design with application to structural vibration control. J. Franklin Inst. 351 (1), 139–155.

Palacios-Quiñonero, F., Rubio-Massegu, J., Rossell, J.M., Karimi, H.R., 2014b. Recent advances in static output-feedback controller design with applications to vibration control of large structures. Modeling, Identification and Control: A Norwegian Research Bulletin 35 (3), 169–190.

Rubió-Massegú, J., Rossell, J.M., Palacios-Quiñonero, F., Karimi, H.R., Oct. 2014. Static output-feedback controller design for vehicle suspensions: an effective two-step computational approach. IET Control Theory & Appl. 8 (15), 1566–1574.

Shieh, L.S., Tsay, Y.T., Yates, R.E., 1983. Block transformations of a class of multivariable control systems to four basic block companion forms. Comput. Math. Appl. 9 (6), 703–714.

Tsui, C.-C., Nov. 1994. A new robust stability measure for state feedback systems. Syst. Contr. Lett. 23 (5), 365–369.

Veselý, V., 2001. Static output feedback controller design. Kybernetika 37 (2), 205–221.

Waltz, R.A., Morales, J.L., Nocedal, J., Orban, D., Jul. 2006. An interior algorithm for nonlinear optimization that combines line search and trust region steps. Math. Program. 107 (3), 391–408.

Wei, C., Zhang, K., Cai, Y., Wang, Z., Yu, W., Mar. 2018. A new method of static output-feedback H_∞controller design for 5 DOF vehicle active suspension system. J. *Braz. Soc. Mech. Sci. Eng.* 40 (3), 1–12.

Wu, Z., Wang, Y., Xiong, J., Xie, M., Feb. 2019. Static output feedback stabilization of networked control systems with a parallel-triggered scheme. ISA (Instrum. Soc. Am.) Trans. 85 (2), 60–70.

Yaici, M., Hariche, K., 2014. On eigenstructure assignment using block poles placement polynomials. Eur. J. Contr. 20 (5), 217–226.

Zhang, Lei, 2016. Simulation of the transient flow in a natural gas compression system using a high-order upwind scheme considering the real-gas behaviors. J. Nat. Gas Sci. Eng. 28 (1), 479–490.

Řezáč, M., Hurák, Z., Dec. 2013. Structured MIMO design for dual-stage inertial stabilization: case study for HIFOO and Hinfstruct solvers. Mechatronics 23 (8), 1084–1093.